scientific reports

Check for updates

OPEN

Combined response of polar magnetotaxis to oxygen and pH: Insights from hanging drop assays and microcosm experiments

Xuegang Mao[1,2]✉, Ramon Egli[3]✉, Nikolai Petersen[4] & Xiuming Liu[1,2]

Magnetotactic bacteria (MTB) combine passive alignment with the Earth magnetic field with a chemotactic response (magneto-chemotaxis) to reach their optimal living depth in chemically stratified environments. Current magneto-aerotaxis models fail to explain the occurrence of MTB far below the oxic-anoxic interface and the coexistence of MTB cells with opposite magnetotactic polarity at depths that are unrelated with the redox gradient. Here we propose a modified model of polar magnetotaxis which explains these observations, as well as the distinct concentration profiles and magnetotactic advantages of two types of MTB inhabiting a freshwater sediment: a group of unidentified cocci (MC), and a giant rod-shaped bacterium (MB) apparently identical to *M. bavaricum* (MB). This model assumed that magnetotactic polarity is set by a threshold mechanism in counter gradients of oxygen and a second group of repellents, with, in case of MB, includes H^+ ions. MTB possessing this type of polar magnetotaxis can shuttle between two limit depths across the redox gradient (redox taxis), as previously postulated for *M. bavaricum* and other members of the *Nitrospirota* group. The magnetotaxis of MB and MC is predominantly dipolar whenever the presence of a magnetic field ensures a magnetotactic advantage. In addition, MB can overcome unfavorable magnetic field configurations through a temporal sensing mechanism. The availability of threshold and temporal sensing mechanisms of different substances can generate a rich variety of responses by different types of MTB, enabling them to exploit multiple ecological niches.

Magnetotactic bacteria (MTB) contain intracellular chains of nano-sized magnetite and/or greigite crystals, which ensure a passive alignment with the Earth's magnetic field B[1,2,3], known as magnetotaxis. Combination of this alignment with the swimming direction determined by surrounding environment (chemotaxis) yields a one-dimensional displacement along magnetic field lines, reducing a three-dimensional search problem of ordinary chemotaxis to one of a single dimension[4]. Magneto-chemotaxis is therefore more efficient than chemotaxis alone in all situations where the component of Balong the sought direction of displacement exceeds few μT[5]. This magnetotactic advantage is also available to MTB living in sediment, despite the poor (~ 1–3%) alignment with Bcaused by the limited space available in sediment pores[6]. Many MTB are sensitive to oxygen through a temporal sensing mechanism and/or a threshold mechanism, whose combination determines a variety of responses known as magneto-aerotaxis[7,8,9]. These sensing mechanisms regulate the frequency with which the swimming direction is changed by reversing the flagellar motor. With axial magneto-aerotaxis, bacteria move towards decreasing (increasing) $[O_2]$, if $[O_2]$ is larger (smaller) than a given upper (lower) threshold, with the dominant direction being chosen through a temporal sensing mechanism. As a result, MTB migrate towards the oxic-anoxic interface (OAI) of stratified environments, where $[O_2]$ is intermediate between the lower and upper thresholds. Dipolar magneto-aerotaxis, on the other hand, relies only on the threshold mechanism. The preferred swimming direction relative to B in a hanging drop assay, where $O_2$is nearly saturated, determines the magnetotaxis polarity, that is, north-seeking (NS) if swimming towards the magnetic North, or south-seeking (SS) otherwise. Most cells retrieved in the northern hemisphere are NS when exposed to large oxygen concentrations and SS in the southern hemisphere, since these polarities makes them swim downwards along the inclined field lines. Equal amounts of NS and SS MTB have been found in proximity of the magnetic equator[10],

[1]Key Laboratory for Humid Subtropical Ecogeographical Processes of the Ministry of Education, Fujian Normal University, Fuzhou 350117, China. [2]Institute of Geography, Fujian Normal University, Fuzhou 350117, China. [3]Department of General Geophysics and Conrad Observatory, GeoSphere Austria, Hohe Warte 38, 1190 Vienna, Austria. [4]Department of Earth and Environmental Sciences, Ludwig-Maximilians University, Theresienstrasse 41, 80333 Munich, Germany. ✉email: maoxuegang1@163.com; ramon.egli@geosphere.at

where the field lines are horizontal. The direction of *B*relative to chemical gradients is therefore considered to be responsible for polarity selection[7,11].

Unipolar magneto-aerotaxis is similar to dipolar magnetotaxis, but a temporal sensing mechanism exists either above an upper [O_2] threshold or below a lower [O_2] threshold[9]. In this case, reversing *B* causes an initial divergence of the cell band, followed by a reversal of the swimming direction for all cells above or below the optimal living conditions, so that all cells end up moving towards or away from O_2. In certain cases, coexisting groups of cells from the same culture show distinct magneto-aerotaxis responses[9]. These observations suggest that axial and polar magnetotaxis might be the idealized endmembers of a range of intermediate responses to chemical gradients. Furthermore, magnetotaxis is also affected by light (phototaxis) and physical contact[12,13,14,15,16]. Non-chemical stimuli might provide additional clues for navigation in the water column and in the sediment. The threshold sensory mechanism might also depend on metabolic states of the cell. A metabolic control of magnetotaxis would have the benefit of avoiding unnecessary displacements[17]; however, fast chemotactic responses are still needed to escape potentially damaging conditions. Cell metabolism is expected to play an important role in redox taxis[17]: for instance, MTB from the *Nitrospirota* phylum accumulate elemental sulfur (S^0) through sulfate reduction while resting in the reducing zone, until a "reduced" internal state triggers the magnetotactic polarity reversal required to move up to the microaerobic zone, where S^0can be oxidized[18]. Complete consumption of S^0 would switch the cell to an "oxidized" state that makes it migrate again to the reduced zone.

Current models of magnetotaxis are challenged by the observation of MTB with opposite magnetotactic polarity coexisting in at the same depths in horizontally stratified water columns, and the lack of a consistent relation between polarity and position in the redox gradient[14,19,20,21]. A second sensory state that does not depend on O_2 is needed to switch the magnetotactic polarity of MTB populations reaching well below the OAI, where O_2can no longer be sensed, albeit such a polarity switching has never been observed in controlled experiments[12]. This goes along with the possible lack of a lower O_2 threshold in some MTB, as suggested hanging drop assays with polar MTB retrieved from the same sediment used in this study. These assays yielded always the polarity expected in the case of O_2saturation, regardless of sampling depth, even when sampling and observations were performed under strictly anoxic conditions and in the dark, using sediment microcosm preserved under these conditions for several months[22].

In the present study, we observe the response of MTB retrieved from sediment to pH gradients, and show, for the first time, that the magnetotactic polarity of MB can be switched by a pH-driven threshold sensing mechanism. Our result suggests that MB's polar magnetotaxis is controlled by at least two substances associated with natural redox gradients. Using results obtained from previous experiments with MTB living in the same sediment[6,22], we extend existing models of polar magneto-aerotaxis and resolve the abovementioned inconsistencies between theory and observations.

Methods

Freshwater sediment was collected using a grab sampler from a small pond (30×7×0.5 m) in Niederlippach, Germany, (48°35′14.98″ N, 12°04′43.71″ E)[22,23], and transferred to glass aquaria that were kept at room temperature in the Earth's magnetic field (Supplementary Fig. 1a, b). A new sediment stratification and oxygen gradient was reestablished after ~ 10 days. After complete stabilization, 3–5 cm long mini cores were taken from the sediment using a plastic drinking straw (diameter: 5 mm) and sliced in 1 mm increments. Each slice was diluted with distilled water (~ 200 µL) and prepared for a hanging drop assay on a rubber O-ring to prevent rapid evaporation (insert of Supplementary Fig. 1c). MTB cells swimming out of the sediment were observed and counted under a special optical microscope[6] equipped with Helmholtz coils for producing a controlled magnetic field (Supplementary Fig. 1c). The quasi totality of MTB observed with this apparatus belonged to two groups: (1) unidentified magnetic cocci (MC) containing one or more chains of prismatic or tooth-shaped magnetosomes (Fig. 1a, b), and (2) a giant rod-shaped bacterium (MB) apparently identical to *M. bavaricum*[24,25] (Fig. 1c, d), which has been previously identified in the same pond[26]. Despite their diversity, all observable MC cells displayed the same magnetotactic behavior and are considered as a single group in this study. The presence of sulfur inclusions (Fig. 1d) in MB cells was confirmed by energy-dispersive X-ray spectroscopy (EDS) (Supplementary Fig. 2).

MTB freshly retrieved from the sediment present strong tactile responses and a tendency to decrease their motility with time, or upon transferring them to another setup once they left the sediment. Attempts to transfer MTB cells into microfluidic devices, where controlled chemical gradients can be created, were not successful. In order to compare our results with previous studies on the displacement of MC and MB in sediment[22], which is essential for understanding how magnetotaxis works under natural conditions, we stuck to the observation of MB retrieved from microcosms using a modified version of the hanging drop assay (Fig. 2a). This assay has been used to observe the motion of MB cells in a pH gradient, under conditions that were as close as possible to the classic hanging drop assay used here as control experiment.

Hanging drops were prepared as follows: ~ 0.5 mL of MTB-containing sediment was taken with a micropipette from an aquarium and transferred to a glass slide (2.6×7.6 cm). Then, ~ 1 mL distilled water (pH 7) was added on the top of the sediment drop to create a clear water rim around the sediment. Placement of a cover glass (2×2 cm) onto the sediment–water preparation creates a thin film of homogeneous thickness. A series of aqueous solutions with pH values ranging from 1 to 12 have been prepared by successive dilution of 1 M HCl or NaOH with distilled water. The pH value of each solution was confirmed with a pH sensor from Unisense. About 0.1 mL of the as-prepared pH solution was deposited onto one side of the cover glass, providing a reservoir that is in contact with the fluid under the cover glass (Fig. 2a). The thin fluid layer below the cover glass prevents turbulent mixing, so that a pH gradient forms by diffusion and propagates toward the other end of the cover glass. This setup does not allow to monitor actual pH values; however, as discussed later, a qualitative assessment

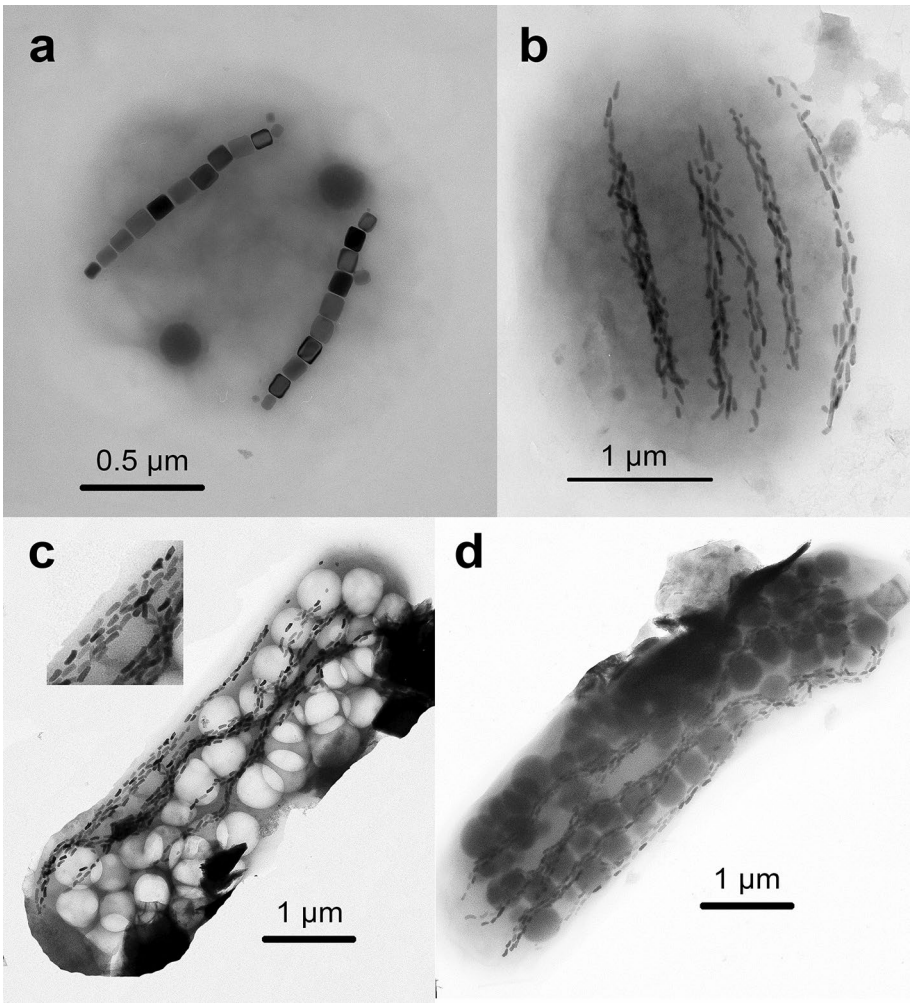

Fig. 1. Transmission electron micrograph (TEM) images of a MC cell containing two chains of prismatic magnetosomes (**a**), and chain strands of tooth-shaped magnetosomes (**b**). TEM images of a MB cell containing empty (**c**) and filled (**d**, arrow) sulfur inclusions. A detail of MB's tooth shaped magnetosomes is shown in the insert of (**c**).

of the pH gradient is sufficient to elucidate the magnetotactic response, which is therefore simply described by the pH value of the added solution.

A rough assessment of the pH gradient is obtained from the solution of the one-dimensional diffusion equation

$$\frac{\partial C}{\partial t} = D\frac{\partial^2 C}{\partial x^2} \tag{1}$$

inside the fluid layer below the cover glass, where $C = C(x, t)$ is the concentration of H^+ or OH^- ions as a function of the distance x from the cover slide edge where the solution was added at the time $t = 0$, and $D \approx 2.3 \times 10^{-9}$ m^2/s is the self-diffusion coefficient of water at room temperature. The initial condition $C(x, t) = C_0\theta(x)$, where C_0 is the concentration of ions and θ is the Heaviside unit step function, describes the addition of the pH solution at $t = 0$. Suitable boundary conditions must be set at $x = 0$ and at the opposed side $x = -L$ of the cover slide ($L \approx 2$ cm). Because the added drop of pH solution is much thicker than the fluid layer under the cover slide, we assume an infinite reservoir with $C(0, t) = C_0$ at $x = 0$. The other end of the cover slide is a physical barrier with no flux, whence $\partial C / \partial x = 0$ for $x = -L$. Numerical solutions of Eq. (1) are shown in Fig. 2b (H^+ ions) and Fig. 2c (pH) for a 2-cm-wide cover slide and a pH 3 solution ($[H^+]_0 = 10^{-3}$). These solutions show that a pH front with decreasing sharpness propagates under the cover slide for the first ~ 30 min. During this time, the left-hand side of the cover slide is unaffected by the pH solution. The pH front disappears completely after 2 h, when the pH of the entire water film starts to decrease until it equilibrates with the added solution. Accordingly, we expect a pH gradient along x to be present during the first ~ 30 min, so that MTB cells exiting the sediment will swim from a near-neutral environment into a < 1 mm-wide diffusion front. All observations were performed within 30 min from preparation, after placing the glass slide under the optical microscope in a controlled magnetic field. Motile cells can be observed for several hours, which means that evaporation is not an issue in these experiments.

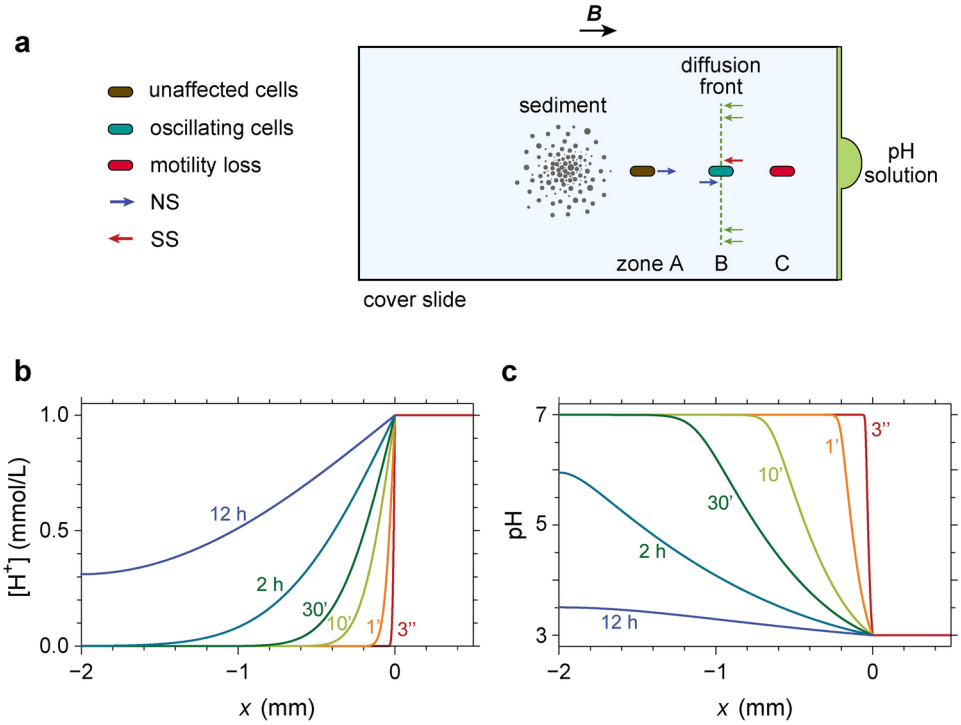

Fig. 2. Hanging drop assays with a pH gradient. (**a**) Setup for observing MTB in a pH gradient (top view and side view, not to scale). See the text for the definition of zones A, B, and C. (**b**, **c**) Simulated profiles of $[H^+]$ and pH in the liquid film under the glass cover, for selected times after the addition of a pH 3 solution at the right end of the cover slide.

Added solution	NS	Oscillating	SS	Full stop (immobile)	Full stop (vibrating)
Control[a]	103 ± 15.3 (98.1%)	2 ± 1.0 (1.9%)	0	0	0
pH 1	0	0	0	60 ± 10.0 (97.6%)	2 ± 0.7 (2.4%)
pH 2[b]	2 ± 0.7 (8.1%)	0	24 ± 7.5 (91.9%)	not observed	not observed
pH 2[c]	2 ± 0.8 (3.3%)	43 ± 6.2 (85.3%)	2 ± 0.0 (4.0%)	4 ± 1.5 (7.4%)	0
pH 3	5 ± 1.7 (7.3%)	59 ± 8.6 (89.9%)	0	2 ± 0.7 (2.7%)	not observed
pH 4	0	0	0	2 ± 1.0 (11.1%)	18 ± 6.8 (88.9%)
pH 5	0	0	0	2 ± 0.6 (8.1%)	19 ± 5.3 (91.9%)
pH 6	1 ± 0.0 (4.5%)	0	0	1 ± 0.6 (6.1%)	20 ± 2.1 (89.4%)
pH 7	28 ± 7.6 (91.9%)	0	0	1 ± 0.0 (3.2%)	2 ± 0.7 (4.9%)
pH 8	2 ± 0.5 (10%)	0	0	0	16 ± 3.6 (90%)
pH 12	0	0	0	79 ± 10.3 (100%)	0

Table 1. Summary of results obtained from hanging drop assays. Numbers indicate cell counts. [a] Standard assay. [b] Before oscillating cells were observed. [c] While oscillating cells were observed.

Results

Control experiments and loss of cell motility

A series of pH solutions (pH 1–12) have been used to test the MTB response to a pH gradient. Experiments with each solution have been repeated at least three times with reproducible results. Addition of a pH 7 solution, which is similar to the near-neutral pH of the sediment used in our experiments[26], did not produce a noticeable change in the swimming behavior of both MTB types with respect to simple hanging drop assays, with cells being consistently NS (Table 1). In rare cases, few (< 1%) MB engaged an oscillatory motion (Movie S1). This control experiment shows that the one-sided addition of an aqueous solution to the hanging drop setup does not modify, per se, the magnetotactic polarity of MB and MC cells.

Nearly all MTB cells lose their motility with a complete stop of the flagellar motor upon adding very acidic (pH 1) or alkaline (pH 12) solutions once they reach the diffusion front (Movie S2). Motility was not resumed

upon reversing and/or rotating the magnetic field. On the other hand, the addition mild solutions (pH 4–6 and 8) triggered a different response, with MB cells slowing down to a full stop after reaching the diffusion front. After stopping, rapid transversal vibrations of the cell body (Movie S3), indicate that the flagellar motor was still active, but flagella were no longer arranged in a way that supported forward propulsion[27]. Transversal vibrations are produced by random torques that would make the cell tumble in the absence of a magnetic field. Tumbling is a typical chemotactic response of motile bacteria[28], which, in the case of MTB, might serve other purposes. Normal swimming was not resumed by reversing or by rotating the magnetic field.

Magnetotactic polarity switching

A distinct pattern that included magnetotactic polarity switching, that is, a reversal of the swimming direction without cell rotation (Movie S4), was observed only in the case of MB cells approaching the pH gradients created by adding moderately acidic solutions (pH 2–3). This pattern is best described by dividing the cover slide into three zones, labeled as A, B, and C, according to the increasing proximity to the side where the solution was added (Fig. 2a). In zone A, which extends from the sediment to a certain distance from the diffusion front, cells maintained the usual NS behavior (Movie S4, 0′4″–0′6″), eventually approaching the pH front. In the pH 2 experiment, few (4.4%) MB cells continued to swim along the same direction until reaching zone C, closest to the side where the solution was added, until the flagellar motor suddenly stopped. Motility could not be resumed by reversing and/or rotating the magnetic field (Movie S4, 0′9″–0′12″), alike the experiments with pH 1 solutions. Most MB cells, however, reversed their swimming direction in zone C, effectively becoming SS (Movie S4, 0′50″–2′10″). These SS cells occasionally reverted to NS for short periods of time (0.5–1 s), however, the net swimming direction was SS (Movie S4, 0′50″–2′10″). The SS motility triggered in zone C did not cease until cells reached again zone B, where they engaged a distinct back-forward motion (referred to as oscillating in the following) by switching their flagellar motor every 0.15–0.6 s, with no systematic bias in favor of either direction (Movie S4, 0′17″–0′33″ and 2′15″–2′22″). The oscillating motion maintained these cells in zone B for several minutes. In the pH 3 experiment, most MB cells engaged the same oscillating motion as soon as they reached zone B (Table 1).

After reversing the magnetic field (Movie S4, 0′33″), MB in zone B stop to oscillate, resuming their normal swimming behavior (Movie S4, 0′33″–0′40″), mostly (~ 91%) with NS polarity, and the remaining part (~ 9%) with SS polarity (Movie S4, 2′41″–2′49″). NS cells eventually reached back into zone A, while SS cells advanced towards zone C. If the original magnetic field direction was restored (Movie S4, 0′42″), both NS and SS cells returned to zone B and engaged the same oscillatory motion observed before (Movie S4, 0′43″–0′46″). If the magnetic field was turned by 90° (Movie S4, 2′53″), all MB cells became NS, stopping the periodic polarity reversal (Movie S4, 2′53″–3′11″). Zeroing the magnetic field made MB cells swim randomly, with no preferred direction (Movie S5 0′2″–0′41″).

Tracking periodic magnetotactic polarity reversals

Detailed insights into the periodic motion of MB cells in zone B have been obtained by digitizing individual swimming paths in Movie S4 (0′29″–0′36″). The first example (Fig. 3a) depicts a large cell that oscillates with an unusually large amplitude. Its swimming path is composed of discrete sections characterized by constant swimming velocities with alternating sign, as deduced from the saw-tooth pattern of the x-coordinate $x(t)$. The y-coordinate, on the other hand, remains nearly constant, up to small random fluctuations, as expected from the strong alignment of MB cells[6] in the ~ 0.1 mT field parallel applied along x. The asymmetry of the saw-tooth pattern is caused by the swimming velocity of SS tracks being ~ 37% smaller than that of NS tracks. Similar differences between field-parallel and antiparallel migration velocities have been observed in capillary assays[9]. This pattern clearly shows that oscillations around a mean position are not random, being caused by flagellar motor reversals occurring at two fixed positions along the pH gradient. Most MB cells in zone B oscillate much more rapidly, as seen in Fig. 3b. In these cases, the rapid (~ 6 Hz) alternation of the swimming direction prevents a precise discrimination between NS and SS velocities. In both examples, the magnetic field was reversed while the cells were NS. Thereafter, cells continued to be NS and swam away from the diffusion front. The last example (Fig. 3c) depicts two oscillating cells that are only ~ 50 μm apart from each other, which means that they move inside the same chemical gradient roughly oriented along x. The field was reversed when both cells were NS, yet one cell remained NS, while the other cell became SS after ~ 0.4 s and swam toward the pH front. Because of identical external conditions, the different behaviors of the two cells must be attributed to cell-internal factors, due for instance to a memory effect[29].

pH sensitivity

The above observations can be summarized as follows: (a) The addition of solutions with pH values close to the natural sedimentary environment (pH 7) did not produce any visible difference with respect to the regular hanging drop assay; (b) the addition of highly acidic or alkaline solutions (pH 1 and 12) led to a complete stop of the flagellar motor once passing through the diffusion front (zone C); (c) the addition of weakly acidic or alkaline solutions (pH 4–6 and 8) led to a progressive slowdown and stop once passing through the diffusion front (zone C), however, the flagellar motor was still active; (d) the addition of moderately acidic solutions (pH 2–3) triggered a magnetotactic polarity reversal in most cells, which led to an oscillatory motion either directly in zone B (pH 3), or after a first reversal in zone C (pH 2); (e) after reversing B, ~ 91% of the oscillating cells revert to their usual NS state, while the remaining ~ 9% becomes SS; (f) reverting B to the original polarity resumes the oscillatory behavior once the cells returned to zone B. Finally, MC cells were either unaffected, or they slowed down and lost their motility upon encountering a sufficiently strong pH gradient (Movie S6), suggesting that pH does not trigger a magnetotactic polarity reversal in this type of MTB.

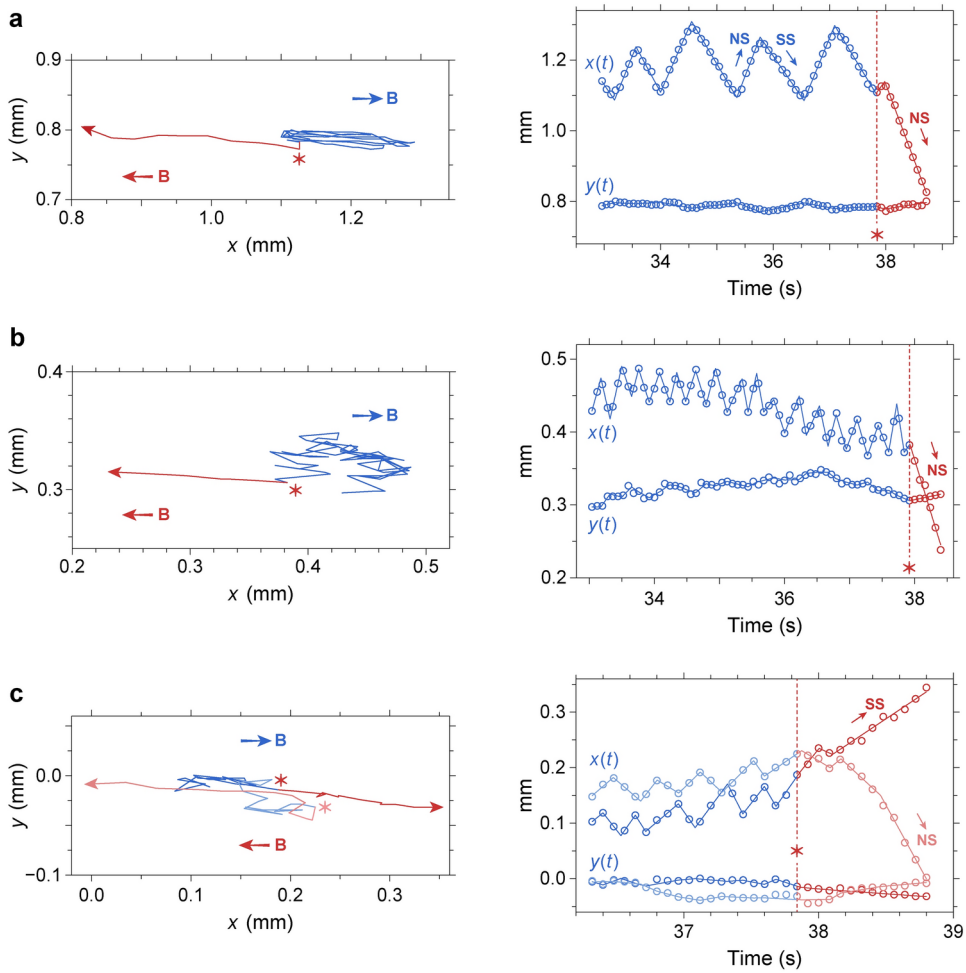

Fig. 3. Oscillatory swimming paths of selected MB cells in the $[H^+]$ gradient created in zone B by the addition of a pH 3 solution. Left plots: swimming paths digitized from Movie S4. Arrows indicate the field direction before and after the field reversal. The point of the path where the reversal occurred is indicated by an asterisk. Right plots: x- and y-coordinates of the digitized paths (circles), as a function of time. The vertical dashed line indicates the field reversal at $t = 37.8$ s. The path coordinates $x(t)$ and $y(t)$ have been fitted with straight segments corresponding to a constant swimming velocity. Before the field is reversed, positive and negative slopes of $x(t)$ represent NS and SS magnetotactic polarities, respectively, while the opposite is true after field reversal. (**a**) Large MB cell performing unusually large oscillations. The asymmetric saw-tooth pattern in $x(t)$ defines the NS and SS swimming velocities $v_{NS} = 0.40 \pm 0.02$ mm/s and $v_{SS} = 0.25 \pm 0.03$ mm/s, respectively, which are switched with a frequency $f = 1.7$ Hz. The cell was NS when the field has been reversed. (**b**) Same as (**a**) for a smaller cell performing faster oscillations ($v_{mean} = 0.33 \pm 0.1$ mm/s, $f = 6.6$ Hz). (**c**) Same as (**a**) for two close cells ($v_{mean} = 0.33 \pm 0.1$ mm/s, $f = 6.4$ Hz). In this case one cell becomes SS when the field is switched, and therefore continues to swim towards the pH front.

Mechanism of pH-driven polar magnetotaxis switching

The periodic swimming direction reversal engaged by MB cells in properly set pH gradients differ from changes of the magnetotactic behavior triggered by other stimuli, such light as tactile responses. For instance, the bounce and ping-pong motion of multicellular magnetotactic prokaryotes (MMPs), which is triggered by UV light (phototaxis) or tactile stimuli[15161718]is irregular and depends on the sampling season, storage time in the laboratory, observation duration, and on the magnetic field strength[30,31]. Our observations, on the other hand, depend on the presence of a pH gradient, this gradient being the only difference with control experiments. The response of MB cells to pH gradients, which enables them to escape very acidic or alkaline conditions, is analogous to that of other neutrophilic bacteria[32,33].

The oscillatory motion of MB in zone B resembles that of spirilla[7,8,11,17,18]. However, the cause is completely different: in absence of an oxygen gradient in the hanging drop assay, the temporal sensing mechanism of spirilla is subjected to random fluctuations and measures essentially noise, triggering swimming direction reversals at random times. The oscillation of MB in zone B, on the other hand, is very regular (Fig. 3). Proximity to zone C, where excessively acidic conditions suppress cell motility, ensures that the concentration of H^+ ions in zone B abundantly exceeds the noise level of the sensory mechanism, so that changes in swimming direction are

triggered deterministically either by a concentration gradient or by a concentration threshold. Our observations might be therefore compared with oscillations of MV-1 and SS-5 cells within the aerotactic band.

In case of spatiotemporal sensing mechanisms[34], cells compare the concentrations $C_1 = C(x(t))$ and $C_2 = C(x(t+\Delta t))$ of a repellent – in our case H^+ ions – along the swimming path $x(t)$ over successive time intervals Δt, therefore effectively sensing a spatial gradient $G(x) = (C_2 - C_1)/v\Delta t$ along x, with $v$being the swimming velocity. In this case, the only role played by the magnetic field is that of determining the axis along which the gradient is sensed, so that the response to a field polarity reversal is purely axial[7]. Our experiments show that the periodic change of the swimming direction by cells that engage an oscillatory motion in zone B ceases immediately after reversing the field polarity, yielding NS or SS cells with the normal swimming behavior observed without a pH gradient. This observation proves that MB cells do not react to pH gradients via a spatiotemporal sensing mechanism.

The threshold sensing model[8]assumes that the swimming direction of MB cells is switched by a threshold concentration detected by external[35]or internal[36] receptors. We assume that the capture of molecules and the transmission of signals to the flagellar motor produces a certain delay between the actual concentration $C(x(t))$ along the swimming path $x(t)$ of the cell, and the sensed concentration $C_s(t)$. This delay might be controlled by a diffusive process[35]or by a reaction rate[37]. To keep the conceptual model as simple as possible, we use a one-dimensional model of tracer diffusion across planar sheet of thickness $2d$ that surrounds the receptors located at $z = 0$. The exact geometry of the problem is irrelevant, because the thickness of the sheet and its diffusion coefficient combine into a single parameter $\tau_d = d^2/D$ which controls the time dependence of the tracer concentration profile $c(z, t)$ across the sheet[38]. With these settings, $C_s(t) = c(z = 0, t)$, where c is the solution of the one-dimensional diffusion equation with boundary condition $c(\pm d, t) = C(x(t))$, and $x(t)$ the swimming path and C the tracer concentration outside the cell. Since d^2/D and the pH profiles of the hanging drop experiments are unknown, all simulations results discussed below are expressed in arbitrary units assuming $D = 1$, $d = 1$, and $v = 1$ without loss of generality.

The initial condition for a cell that just left the sediment and swims towards the diffusion front (zone A) is $C = C_s \approx 0$. The cell is initially NS, so that $x(t) = v_{NS}\, t$, where $v_{NS} > 0$ is the NS swimming velocity. In zone B, $C(x(t))$ starts to increase, and the same occurs for $C_s(t)$ with some delay caused by diffusion across d (Fig. 4a). When $C_s(t)$ reaches a critical threshold C_s^* (assumed to be 0.2 in the unitless simulations of Fig. 4), the swimming direction is reversed and the cell becomes SS, moving back towards the starting point. C_s initially continues to increase while C is decreasing, but the trend is inverted after passing the point where $C_s = C$. If the cell remains SS, C_s will eventually cross a threshold that makes the cell becoming NS again. For convenience, we assume this threshold to be identical to C_s^*. While the cell is moving again towards the repellent, C_s continues to decrease for a while, until the increase of C reverses this trend. At a certain point, C_s exceeds C_s^* a second time, and the cell becomes SS. This cycle is repeated indefinitely, as long as $C(x)$ is constant, yielding the periodic functions $x(t)$, $C(x(t))$ and $C_s(t)$ of Fig. 4b. The periodicity of $x(t)$ represents the oscillatory behavior of the cell around a mean position close to the point where $C = C_s^*$.

The qualitative characteristics of the periodic motion depend only on the existence of (a) a sensed threshold C_s^* that triggers a magnetotactic polarity reversal and determines the mean position of the cell with respect to the pH gradient, and (b) a delay between C and C_s, which controls the period $\sim d^2/D$of the oscillatory motion. Sensing mechanisms depend in a complex manner on the external input and its past evolution, generating hysteretic responses that reduce the flagellar motor chatter in case of concentrations close to the noise level[39]. As a result, the response is apparently controlled by two thresholds $C_{1,2}$of the external concentration[40], depending on whether the sensed concentration increases (C_0), or decreases ($C_1 < C_0$) in time. The sensory mechanism itself might possess two different internal thresholds, as it has been postulated for $[O_2]$ in magneto-aerotaxis[7,9]. Addition of a second internal threshold $> C_s^*$ in the above model moves the NS→SS turning point further to the right, making the cycle depicted in Fig. 4a,b more symmetric. Cells, however, would continue to oscillate between two points of the unknown pH gradient.

The above model also explains the response of oscillating cells to a field polarity reversal. Figure 4c–f depicts four cases where the field polarity is reversed at different points of the cell trajectory: two cases when the cell is NS and two cases when the cell is SS. Depending on the instantaneous value of C_s during the field polarity reversal and the subsequent evolution of C_s while the cell is swimming in the opposite direction, the magnetotactic polarity might or might not be switched another time. The outcome is either a NS cell in the reversed field, which moves away from the repelling zone, or a SS cell in the reversed field, which swims towards the repelling zone. Because oscillating cells spend most of their time in a region where the repellent concentration is $< C_s^*$, the probability to end in a SS state after field reversal is much lower than that of ending in a NS state. This probability is exactly reflected by our observations of MB cells in zone B, with ~ 9% of all oscillating cells becoming SS in the reversed field. The evident disproportion between NS and SS cells produced by the field reversal indicates that the magnetotactic polarity is switched by a single internal threshold or by two similar ones, since the symmetric cycle produced by largely different thresholds gives a 50% chance for either polarity.

Chemotactic response rescaling

Chemotactic sensory systems rescale their response sensitivity (adaptation) so to sense small concentrations differences at concentration levels ranging over several orders of magnitude[41,42,43]. Accordingly, chemotactic responses are triggered by a minimum relative concentration change with respect to a background concentration. The adaptation process takes some time ranging from seconds to minutes[44]and is sensitive to both the sign and the rate of concentration changes[45]. The adaptation and de-adaptation process of motile non-magnetotactic bacteria such as *E. coli*is reflected by the frequency of tumbling intervals, defined as intervals of random cell rotation obtained by reversing the flagellar motor[46]. A different type of adaptation can be observed in the hanging drop experiments performed with a pH 2 solution. In this case, most MB cells will first swim to zone C, where

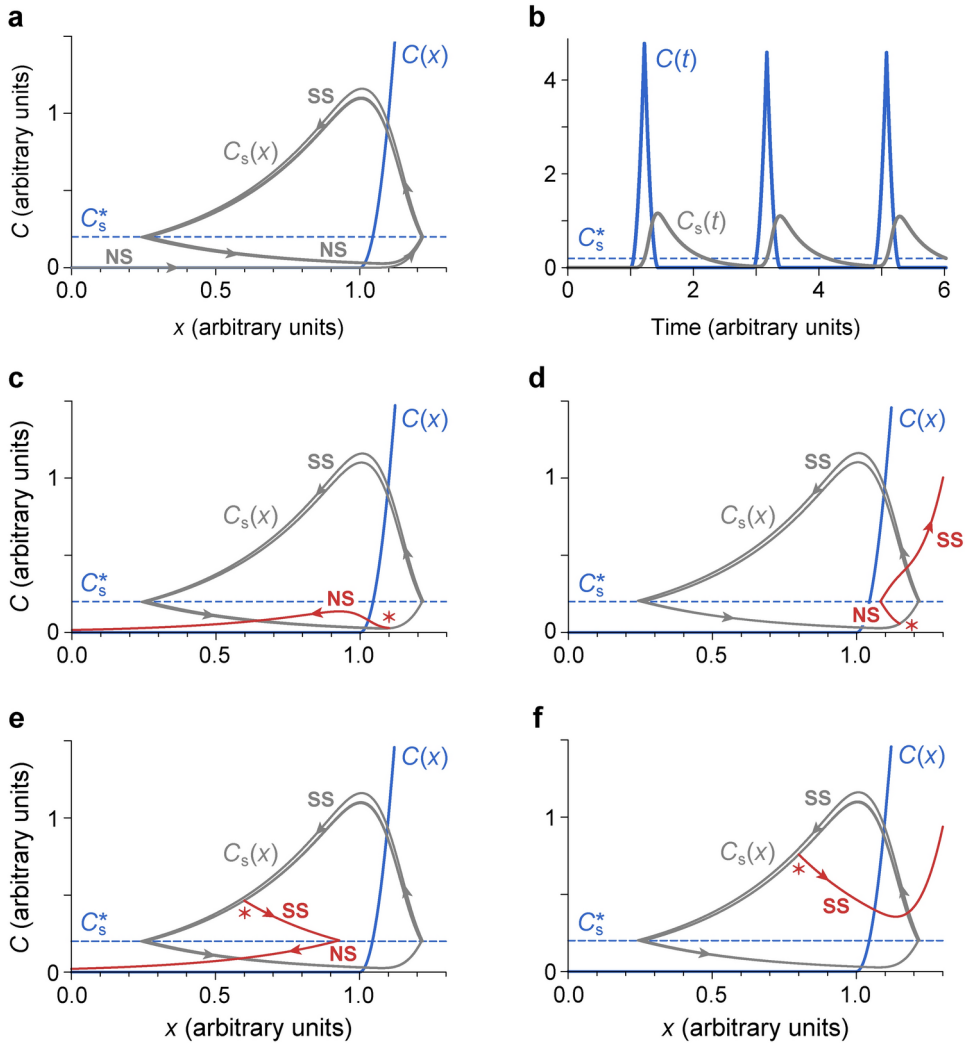

Fig. 4. Numerical simulations of the oscillatory swimming pattern of MB in zone B, according to threshold model explained in the text. All diagrams except (b) represent solutions for a fixed H^+ concentration profile $C(x)$ along x, taken from the solution of the diffusion equation in the fluid layer below the cover slide. (**a**) A NS cell starting at $x = 0$ swims with constant velocity along $+x$ and enters the zone $x > 1$ where $C(x) > 0$. The sensed concentration $C_s(t)$ starts to increase with a delay caused by internal diffusion (gray line with arrow indicating the swimming direction), until it reaches a threshold C_s^* that makes the cell become SS and swim back along $-x$. C_s continues to increase and then slowly decreases as the repelling zone is left. When $C_s = C_s^*$, the cell becomes again NS and the cycle is repeated. (**b**) Same as (a), as a functions of time. (**c**–**f**) Same as (a), when the magnetic field is switched from $+x$ to $-x$ at a point marked with an asterisk. C_s after the field reversal is shown in red. In (**c**, **d**) the field is reversed while the cell is NS: in (*C*) this occurs at a point where C_s is sufficiently small and no longer exceeds C_s^*. In this case, the cell remains NS and swim away from the repellant front in the reversed field. In (**d**), C_s^* is eventually exceeded, and the cell becomes SS. Because the field is reversed, it will swim further towards $+x$ and higher repellant concentrations. In (**e**, **f**) the field is reversed while the cell is SS: in (**e**) this occurs at a point where C_s is sufficiently small to decay below C_s^* before the repellent zone is entered, so that the cell becomes NS and swim away from the repellent front in the reversed field. In (**f**), C_s does not decay below C_s^* before the repellent zone is entered, so that the cell remains SS and swims further towards $+x$.

they become SS, and then swim back to zone B, where they engage in periodic magnetotactic polarity reversals around a mean position. This behavior implies that the first NS→SS trigger in zone C occurs at a much larger H^+ concentration than the subsequent triggers in zone B. The associated threshold change can be explained by the initial adaptation of the sensory mechanism to the concentration increase above the background level of zone A. A delay of few seconds, roughly corresponding the time required to move from zone B to zone C, explains why all cells swim to zone C and lose their motility when stronger pH gradients are used: in these cases, tolerable H^+ concentrations are exceeded before the sensory mechanism can adapt. This does not occur with a pH 3 solution, probably because the gradient formed in this case is shallow enough for the sensory mechanism to switch the flagellar motor already in zone B. We could not measure the instantaneous pH value that causes a motility loss

in our experimental setting, however, as a term of comparison, the flagellar motor of *E. coli*is completely stopped in an external pH of 5[47].

Intermediate responses

The response of MB cells to the addition of mildly acidic or alkaline solutions consisted in an initial slowdown of the flagellar motor, as shown by the decreasing NS swimming speed (Movie S3), followed by a reversal. The reversed rotation speed was not sufficient to sustain the backward motion observed in SS cells obtained with the other experiments. Some studies indicate that the speed of the flagellar motor can be modulated by a variety of molecular mechanisms when circumstances call for a less vigorous motility[48]. In our experiments, this slowdown might represent a reduced response to weak repellent concentrations. Because cell tumbling is prevented by the magnetic torque, slower flagellar rotation in "backward" mode might be used to stop cell motion under conditions where a displacement is not useful.

Discussion

Dipolar magnetotaxis in a countergradient

Results of our modified hanging drop assay show, for the first time, that the magnetotactic polarity can be reversed by an acidic pH gradient through a threshold mechanism. Under the saturated oxygen concentrations of the experiments (~ 220 μM), the critical pH threshold appears to be comprised between 3 and 4 (Table 1). Other experiments conducted with the same microcosms from which MB and MC have been retrieved provide complementary information about the magnetotactic behavior of these bacteria (Table 2). Firstly, a lower [O_2] threshold capable of reversing the NS swimming direction of MB could not be detected, as shown by hanging drop assays conducted under strictly anoxic conditions with MTB retrieved from microcosms hold under the same conditions[22]. On the other hand, experiments show that MB and MC bacteria that were displaced from their preferred living depth could migrate both upwards and downwards in sediment and return to the original depth distribution[22], which means that the magnetotactic polarity must be switchable to SS in both groups. Same experiments conducted with reversed *B*, on the other hand, led to a complete disappearance of MC, and to a drop of the MB population with limited recover of the original depth distribution. Altogether, these results prove the in-situ polar or dominantly polar nature of their magnetotaxis, and the existence of two at least two chemical thresholds, one nearer to the sediment–water interface, which sets the NS state, and a deeper one for setting the SS state. These thresholds must be located within the depth range of living cells, which, in the case of MB, reaches far below the oxygen gradient (i.e., down to > 25 mm, while the oxygen concentration drops below measurable levels at 4 mm depth). In this case, NS → SS switching cannot be triggered by a lower oxygen threshold, as required by polar magneto-aerotaxis models[9], thus requiring a different substance for triggering.

A minimalistic model for the polar magnetotaxis of MB requires a threshold mechanism that is sensitive to at least two substances forming a countergradient in a horizontally stratified environment: one triggering downward swimming along the local inclined field (e.g., O_2) and one triggering upward swimming in the same field (e.g., H^+). The high [H^+] threshold observed in the hanging drop assay (pH ~ 3.5 compared to pH > 6.5 in sediment[26]) can be explained by the fact that the pH gradient coexisted with O_2saturation, unlike the natural stratification of sediment, where the pH changes at much lower oxygen concentrations[26]. Because competing chemotactic stimuli are integrated into a single response, larger H^+ concentrations are needed to overcome the strong stimulus from O_2saturation in the hanging drop assay. Assuming for instance an additive and independent response to multiple stimuli[49], the pH ~ 3.5 threshold in the hanging drop assay would rescale to pH ~ 6.5 in 1% oxygen saturation. Adaptation of the response sensitivity and overlap with other responses might further offset the pH threshold.

Other responses

The in-situ response of sedimentary MC and MB populations to $B = 0$ or to a reversed *B*reveals further details about the coexistence of multiple forms of magneto-chemotaxis. Unlike MC, MB can return to its optimal depth range after being displaced in zero field, albeit in a less efficient manner, meaning that it can use chemotaxis for vertical migration in sediment[22]. Limited MB migration capabilities are observed even after reversing *B*.

Property	Result (MC)	Result (MB)
Dipolar magnetotaxis	Yes (2, 4, 8, 9, 10)	Yes (2, 4, 8, 9, 11, 14)
NS trigger	O_2 (2, upper threshold)	O_2 (2, upper threshold)
SS trigger	Unknown. Maybe lower O_2 by threshold or temporal sensing (transient response in 6)	Lower oxygen threshold does not exist or is strongly suppressed (6), pH (14)
Non-tactile stop with active flagellar motor (tumbling if $B = 0$)	No (14)	Yes (14)
Needs magnetotaxis to maintain depth distribution in undisturbed sediment	No, or only marginally (3)	Yes (3), probably because of redox taxis
Needs magnetic field to regain preferred depth in sediment when displaced	Yes, through polar magnetotaxis (9, 10, 12, 13)	No. Can rely on chemotaxis (3) albeit less efficiently
Can override incorrect field orientations (e.g., through a temporal sensing mechanism)	No (8, 10, 13)	Yes (8, 10, 13) albeit much less efficiently
Perform redox taxis	No (1, 3)	Yes (1, 3)

Table 2. Characteristics of polar magnetotaxis deduced from microscope observations and from microcosm experiments. Numbers refer to individual experimental results listed in Supplementary Table S1.

A temporal sensing mechanism is needed to explain both observations. The combination of threshold and temporal sensing mechanisms within the same bacterial strain has been previously documented[9]. Long-term exposure of undisturbed MC and MB populations in microcosms exposed to $B=0$ did not lead to a significant population decrease in the case of MC, while MB was reduced by ~ 50%[22,50] (Table 2). The depth distribution widened slightly for both groups[22]. A similar long-term experiment where the polarity of B was reversed every day, on the other hand, led to similar cell counts as in $B=0$ for MB, while MC disappeared almost completely. Furthermore, the depth distribution of MB widened significantly and became evidently bimodal. This widening can be explained by cells swimming in the wrong direction during days where $B$was reversed, similarly to what is observed in capillary tubes with MTB performing dipolar magnetotaxis[9].

In summary, dipolar magnetotaxis (i.e., the form of polar magnetotaxis relying only on a threshold mechanism) appears to be always dominant in MC and MB if a correctly configured B is present, while only MB can rely on a temporal sensing mechanism if B does not provide a magnetotactic advantage (i.e., B reversed or horizontal, Table 2). The difference between long-term field exposure experiments and in-situ migration experiments clearly indicate that MC and MB use polar magnetotaxis for different scopes. Maintaining a preferred depth in resting sediment requires only to compensate for the slow solid diffusion caused by small benthic organisms (visible from the burrowing traces). Chemotaxis, albeit less efficient than magnetotaxis, can serve this purpose as well, explaining the relative insensitivity of undisturbed MC populations to $B=0$. On the other hand, MTB that need to shuttle continuously across a chemical gradient through redox taxis, as postulated for *M. bavaricum*[18], require an efficient mechanism that sustains long-distance migration in sediment with minimum energy consumption. Removal of the magnetotactic advantage by cancelling B over long periods of time is thus expected to affect MTB that perform redox taxis more than those that just require to maintain themselves within a preferred depth range. This is indeed observed in the case of MB.

A redox-taxis model for the depth distribution of MB

The threshold response of MB to O_2 and H^+ implies that the swimming direction of dipolar magnetotaxis is switched by the combined stimuli of different substances in a redox countergradient, rather than two distinct $[O_2]$ thresholds as it is the case for polar magneto-aerotaxis models. In the following, we thus consider a redox countergradient made by oxidizing substances whose concentration [Ox] decreases with depth, and reducing substances whose concentration [Red] increases with depth (Fig. 5a). Let R_{ox} and R_{red} at depths z_{ox} and z_{red} be the concentration thresholds above which the magnetotactic polarity of upward-seeking (US) cells and downward-seeking (DS) cells, respectively, is switched. In the northern hemisphere, US and DS are equivalent to SS and NS, respectively. If $z_{ox} < z_{red}$, cells always possess a well-defined magnetotactic polarity, regardless of depth, provided that the magnetotactic polarity set by the R_{ox} threshold is maintained for as long as the R_{red} threshold is not exceeded, and vice versa (Fig. 5a), consistently with the observed lack of a lower $[O_2]$ threshold

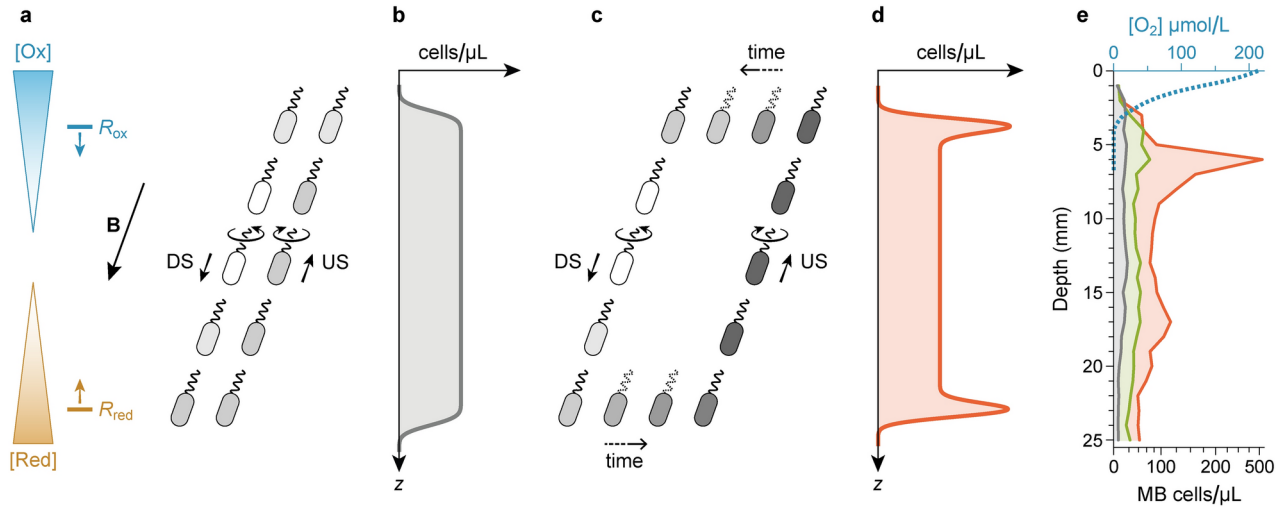

Fig. 5. Model of two-threshold polar magnetotaxis with non-overlapping repellent counter gradients. (**a**) Repellent concentrations [Ox] and [Red] (shaded) and corresponding magnetotactic polarity switching thresholds R_{ox} and R_{red}. **B** represents the inclined field lines in the northern hemisphere. MTB are set to a DS and to an US state at the R_{red} and at the R_{ox} thresholds, respectively, making the cells shuttle along **B**, between two limiting depths defined by the thresholds. The magnetotactic polarity is determined by CCW or CW flagellar rotation. Cell shading indicates the progress of metabolic processes performed under reducing (darkening) and oxidizing (lightening) conditions. (**b**) Idealized cell concentration profile corresponding to (**a**). (**c**) Same as (**a**), for the case where cells pause near the R_{red} and R_{ox} thresholds. (**d**) Cell concentration profile corresponding to (**c**). (**e**) Measured oxygen concentration (dashed line) and MB concentration profiles (solid lines) in sediment (data from ref. 22). The three MB profiles correspond to the average of individual measurements with depth-integrated total concentrations $N < 450$ cells/mm^2 (lowest curve), $N > 1500$ cells/mm^2 (highest curve), and $450 < N < 1500$ cells/mm^2 (intermediate curve).

in MB[22]. In the configuration of Fig. 5a, a cell initially located above z_{ox} will be set into a DS state that produces a downward migration, until z_{red} is reached. At this point, the cell will be set into an US state, and the migration direction is reversed, until z_{ox} is reached again and the cycle is repeated. As a result, cells shuttle continuously between z_{ox} and z_{red}, as postulated by the redox taxis model[17,18]. Under stationary environmental conditions, MTB pauseless shuttling between z_{ox} and z_{red} will be homogeneously distributed between these limiting depths, yielding a uniform cell density profile proportional to the box function $\Pi((z-z_{red})/(z-z_{ox}))$, with $\Pi(x)=1$ for $0\le x\le 1$, and $\Pi(x)=0$ otherwise. Because of unavoidable environmental and phenotypic heterogeneities, z_{ox} and z_{red} are not sharp boundaries, so that a more realistic representation of the expected concentration profile is given by a smoothed version of the box function, obtained by convolving $\Pi(x)$ with a bell-shaped distribution $g(x)$ of z_{ox} and z_{red} values (Fig. 5b).

If redox taxis is used to satisfy different metabolic requirements across the redox gradient[18], it is reasonable to assume that cell migration is paused at the limiting horizons z_{ox} and z_{red} for the time required to complete chemical reactions associated with redox cycling (Fig. 5c). In this case, two peaks of the form $g(z-z_c)\,T_c v/(z_{red}-z_{ox})$, centered at $z_c=z_{ox}$ and $z_c=z_{red}$, respectively, reproduce the concentration profiles of pausing cells, which overlap with the box-shaped distribution of migrating cells (Fig. 5d). The factor $T_c v/(z_{red}-z_{ox})$ corresponds to the ratio between the time T_c spent at z_c and the time spent between z_{red} and z_{ox}, respectively. The total numbers N_{ox} and N_{red} of cells pausing at z_{ox} and z_{red}, respectively, as well as the proportion of DS and US polarities of migrating cells, are dictated by the population balance equations.

$$\begin{aligned}\frac{dN_{ox}}{dt} &= (k_{ox}-\varphi_{ds})N_{ox}+\varphi_{us}\eta_{us}N_{red}\\ \frac{dN_{red}}{dt} &= (k_{red}-\varphi_{us})N_{red}+\varphi_{ds}\eta_{ds}N_{ox}\end{aligned} \tag{2}$$

where k_{ox}, k_{red} are the cell growth rates, φ_{ds}, φ_{us} the fractions of pausing cells that resume DS and US migration per unit of time, and η_{ds}, η_{us} the fractions of migrating cells that reach the target layer, escaping, for instance, predation (see Supplementary Information for details). Stationary solutions ($dN_{ox}/dt=dN_{red}/dt=0$) exist only if $\varphi_{ds}>k_{ox}$, $\varphi_{us}>k_{red}$, and $\varphi_{ds}\varphi_{us}\eta_{ds}\eta_{us}=(\varphi_{ds}-k_{ox})\,(\varphi_{us}-k_{red})$. In this case, the fractions $p_{us}(z_{ox})=(\varphi_{ds}-k_{ox})/(2\varphi_{ds}-k_{ox})$ and $p_{us}(z_{red})=\varphi_{us}/(2\varphi_{ds}-k_{red})$ of US cells near z_{ox} and z_{red} take values comprised between 0 and 50%, and between 50 and 100%, respectively. Exactly 50% of all migrating cells are US, regardless of depth (Fig. 5b) in case of negligible grow rates at ($k_{ox}/\varphi_{ds}=k_{red}/\varphi_{us}=0$). More generally, $p_{us}(z)$ can be any function comprised between 0 and 100% if the population is not stationary, which means that the in-situ magnetotactic polarity of migrating cells is not systematically related to the redox conditions, as previously observed[19,20,21].

The above model explains MB concentration profiles measured over several months[22,50]. The shape of these profiles depends systematically on the depth-integrated cell concentration N, which ranges from <10 to >1800 cells/mm^2. The average of MB profiles with $N<450$ cells/mm^2 is nearly constant between $z_1\approx 3$ mm and $z_2\approx 17$ mm (Fig. 5e), resembling the theoretical box function expected from pauseless shuttling between two limit depths (Fig. 5b). The concentration plateau increases with N and remains within the same limit depths up to $N\approx 1500$ cells/mm^2. Two distinct peaks, centered at $z_1\approx 6$ mm and $z_2\approx 17$ mm, respectively, emerge for the average of profiles with $N>1800$ cells/mm^2. This average resembles the concentration profile predicted for cells that pause at both limit depths (Fig. 5d). The upper peak is comprised between $z\approx 4$ mm, which is the depth where oxygen drops to zero, and ~ 10 mm, while the less pronounced lower peak is slightly broader. The two peaks occur independently of each other, as seen from individual profiles featuring only one maximum that coincides with the upper or the lower peak position (Fig. 6).

Conclusions

Several observations about the magnetotactic behavior of natural MTB that are incompatible with magneto-aerotaxis models can be explained by forms of polar magnetotaxis where magnetotactic polarity is controlled by at least two different substances with opposed concentration gradients through a single threshold sensing mechanism. The first substance (O_2) triggers the polarity that makes cells swim downwards (DS), as expected from magneto-aerotaxis models. The second substance (e.g., H^+) triggers the opposite polarity (US). We were able, for the first time, to observe a systematic magnetotactic polarity switching of MB cells, from DS to US and vice-versa, under the combined action of O_2 and a pH gradient. In our experiments, acidic conditions acted as a repellent, which, in the chemical stratification of the sediment from which MB was retrieved, forms a counter gradient with respect to oxygen. The response of MB cells to mildly acidic or alkaline conditions includes a slowdown of the flagellar motor and subsequent reversal that is compatible with tumbling in the chemotaxis of non-magnetic bacteria. The magnetotactic polarity of MC could not be reversed by a pH gradient, demonstrating the different chemotactic response of these two MTB populations. We could also show that MB can rely on a temporal sensing mechanism to navigate in absence of a magnetic field or in cases where the magnetic field orientation relative to the chemical gradient is unfavorable, while this is not the case for MC. Finally, a detailed analysis of the depth distribution of MB and its temporal variability supports the previously postulated redox taxis model for *M. bavaricum*. A simple magnetotactic mechanism that can support redox taxis is presented with Eq. (2).

The availability of threshold and temporal sensing mechanisms of different substances, along with adaptation[42,43,44]and metabolism-controlled chemotaxis[51], can generate a rich variety of responses by different types of MTB, enabling them to exploit multiple ecological niches. This concept is best exemplified by the differences in depth distribution, migration ability, magnetotactic advantage, and chemotactic responses of MB and MC populations living inside the same sediment. Chemotactic responses that do not involve oxygen might

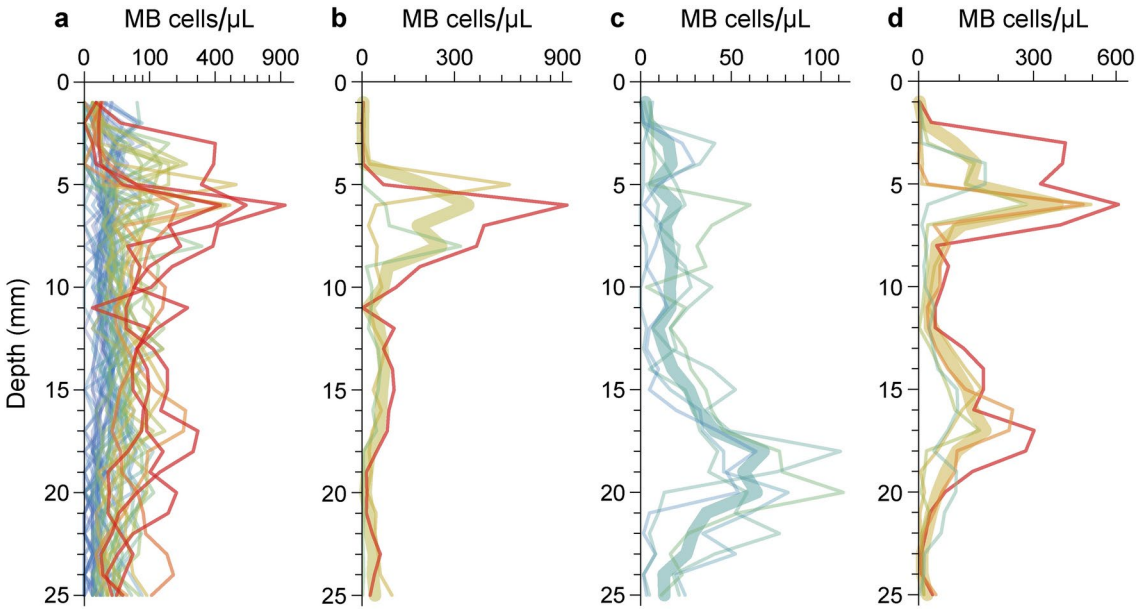

Fig. 6. Variability of MB profiles in a sediment microcosm (data from ref. 22). (**a**) Forty-four individual profiles taken with 1 mm resolution over several months. Lines are color-coded according to the depth-integrated cell concentration, from blue (lowest) to red (highest). Notice the nonlinear scale used to represent profiles with amplitudes that vary over two orders of magnitude. (**b**–**d**) Same as (**a**) for selected profiles with pronounced upper peak, lower peak, and both. The thick line is the average of the plotted profiles.

have played an important role for supporting navigation of phylogenetically deep-branching MTB, of which MB is an example, in ancient anoxic environments, such as the Archean oceans[52].

Data availability

The datasets used and/or analysed during the current study available from the corresponding author on reasonable request.

Received: 24 April 2024; Accepted: 5 November 2024
Published online: 09 November 2024

References

1. Blakemore, R. P. Magnetotactic bacteria. *Annu. Rev. Microbiol.* **190**, 217–238 (1975).
2. Faivre, D. & Schüler, D. Magnetotactic bacteria and magnetosomes. *Chem. Rev.* **108**, 4875–4898 (2008).
3. Lefèvre, C. T. & Bazylinski, D. A. Ecology, diversity, and evolution of magnetotactic bacteria. *Microbiology and Molecular Biology Reviews* **77**, 497–526 (2013).
4. Frankel, R. B. Magnetic guidance of organisms. *Annual review of biophysics and bioengineering* **13**, 85–103 (1984).
5. Bennet, M. et al. Influence of magnetic fields on magneto-aerotaxis. *PLoS ONE* **9**, e101150 (2014).
6. Mao, X., Egli, R., Petersen, N., Hanzlik, M. & Zhao, X. Magnetotaxis and acquisition of detrital remanent magnetization by magnetotactic bacteria in natural sediment: First experimental results and theory. *Geochemistry Geophysics Geosystems.* **15**, 255–283 (2014).
7. Frankel, R. B. & Bazylinski, D. A. Magnetosomes and magneto-aerotaxis. In *Collin M* (ed. Schuch, R.) 182–193 (Karger, 2009).
8. Frankel, R. B., Bazylinski, D. A., Johnson, M. S. & Taylor, B. L. Magneto-aerotaxis in marine coccoid bacteria. *Biophys. J.* **73**, 994–1000 (1997).
9. Lefèvre, C. T. et al. Diversity of magneto-aerotactic behaviors and oxygen sensing mechanisms in cultured magnetotactic bacteria. *Biophysical journal.* **107**, 527–538 (2014).
10. Frankel, R. B., Blakemore, R. P. & F.F. Torres De.Araujo, D.M. Esquivel, and J. Danon.,. Magnetotactic bacteria at the geomagnetic Equator. *Science.* **212**, 1269–1270 (1981).
11. Zhang, W.-J., Chen, C., Li, Y., Song, T. & Wu, L.-F. Configuration of redox gradient determines magnetotactic polarity of the marine bacteria MO-1. *Environ. Microbiol. Rep.* **2**, 646–650 (2010).
12. Zhang, W. J. & Wu, L. F. Flagella and Swimming Behavior of Marine Magnetotactic Bacteria. *Biomolecules.* **10**, 1–14 (2020).
13. Qian, X.-X. et al. Light affects the magnetotactic behaviour and reproduction of ellipsoidal multicellular magnetoglobules in the Mediterranean Sea. *Chinese Journal of Oceanology and Limnology.* **39**, 2005–2014 (2021).
14. Shapiro, O. H., Hatzenpichler, R., Buckley, D. H., Zinder, S. H. & Orphan, V. J. *Multicellular photo-magnetotactic bacteria. Environ. Microbiol. Rep.* **3**, 233–238 (2011).
15. Wenter, R., Wanner, G., Schüler, D. & Overmann, J. Ultrastructure, tactic behaviour and potential for sulfate reduction of a novel multicellular magnetotactic prokaryote from North Sea sediments. *Environmental Microbiology.* **11**, 1493–1505 (2009).
16. Keim, C.N., D.M. da Silva, R.D. de Melo, D. Acosta-Avalos, M. Farina, and H.L. de Barros. 2021. Swimming behavior of the multicellular magnetotactic prokaryote 'Candidatus Magnetoglobus multicellularis' near solid boundaries and natural magnetic grains. *Antonie van Leeuwenhoek*. 0123456789.
17. Bazylinski, D. A., C. T. Lefèvre, D. Schüler. 2013. Magnetotactic bacteria. In: E. Rosenberg et al. (eds.), The Prokaryotes – Prokaryotic Physioligy and Biochemistry, Springer, 453–494.

18. Li, J., P. Liu, J. Wang, A. P. Roberts, Y. Pan (2020). Magnetotaxis as an adaptation to enable bacterial shuttling of microbial sulfur and sulfur cycling across aquatic oxic-anoxic interfaces, *J. Geophys. Res.: Biogeosci.* 125: e2020JG006012.
19. Simmons, S. L., Bazylinski, D. A. & Edwards, K. J. South-seeking magnetotactic bacteria in the Northern Hemisphere. *Science.* **311**, 371–374 (2006).
20. Leão, P. et al. North-seeking magnetotactic gammaproteobacteria in the Southern Hemisphere. *Applied and Environmental Microbiology.* **82**, 5595–5602 (2016).
21. Monteil, C. L. et al. Ectosymbiotic bacteria at the origin of magnetoreception in a marine protist. *Nature Microbiology.* **4**, 1088–1095 (2019).
22. Mao, X., Egli, R., Petersen, N., Hanzlik, M. & Liu, X. Magneto-chemotaxis in sediment: First insights. *PloS ONE.* **9**, E102810 (2014).
23. He, K. et al. Seasonal Variability of Magnetotactic Bacteria in a Freshwater Pond. *Geophysical Research Letters.* **45**, 2294–2302 (2018).
24. Spring, S. et al. Dominating role of an unusual magnetotactic bacterium in the microaerobic zone of a freshwater sediment. *Appl. Environ. Microbiol.* **59**, 2397–2403 (1993).
25. Jogler, C. et al. Conservation of proteobacterial magnetosome genes and structures in an uncultivated member of the deep-branching Nitrospira phylum. *Proc. Natl. Acad. Sci. U. S. A.* **108**, 1134–1139 (2010).
26. Jogler, C. et al. Cultivation-independent characterization of "Candidatus Magnetobacterium bavaricum" via ultrastructural, geochemical, ecological and metagenomic methods. *Environ. Microbiol.* **12**, 2466–2478 (2010).
27. Steinberger, B., Petersen, N., Petermann, H. & Weiss, D. G. Movement of magnetic bacteria in time-varying magnetic fields. *J. Fluid Mech.* **273**, 189–211 (1994).
28. Saragosti, J., P. Silberzan, A. Buguin. 2012. Modeling *E. coli* tumbles by rotational diffusion. Implications for chemotaxis. *PLoS ONE* 7: e35412.
29. Gosztolai, A. & Barahona, M. Cellular memory enhances bacterial chemotactic navigation in rugged environments. *Communications Physics* **3**, 47 (2020).
30. Keim, C.N., J.L. Martins, H. Lins de Barros, U. Lins, and M. Farina. 2006. Structure, behavior, ecology and diversity of multicellular magnetotactic prokaryotes. In: Schüler D, editor. Magnetoreception and magnetosomes in bacteria. Springer-Verlag Berlin Heidelberg.
31. Greenberg, M., Canter, K., Mahler, I. & Tornheim, A. Observation of magnetoreceptive behavior in a multicellular magnetotactic prokaryote in higher than geomagnetic fields. *Biophys. J.* **88**, 1496–1499 (2005).
32. Padan, E., Zilberstein, D. & Schuldiner, S. pH homeostasis in bacteria. *Biochim. Biophys. Acta.* **650**, 151–166 (1981).
33. Tohidifar, P., Plutz, M. J., Ordal, G. W. & Rao, C. V. The mechanism of bidirectional pH taxis in Bacillus subtilis. *Journal of Bacteriology.* **202**, 1–16 (2020).
34. Keller, E. F. & Segel, L. A. *Model for chemotaxis. J. theor. Biol.* **30**, 225–234 (1971).
35. Berg, H. C. & Purcell, E. M. Physics of chemoreception. *Biophys. J.* **20**, 193–219 (1977).
36. Kihara, M. & MacNab, R. M. Cytoplasmic pH mediates pH taxis and weak-acid repellent taxis of bacteria. *Journal of Bacteriology* **145**, 1209–1221 (1981).
37. Block, S. M., Segall, J. E. & Berg, H. C. Adaptation kinetics in bacterial chemotaxis. *Journal of Bacteriology* **154**, 312–323 (1983).
38. Crank, J. *The mathematics of diffusion* (Clarendon Press, 1975).
39. Patnaik, P. R. Noise in bacterial chemotaxis: Sources, analysis, and control. *BioScience* **62**, 1030–1038 (2012).
40. Bhattacharya, S. & Iglesias, P. A. The threshold of an excitable system serves as a control mechanism for noise filtering during chemotaxis. *PLoS ONE* **13**, e0201283 (2018).
41. Vladimirov, N. & Sourjik, V. Chemotaxis: how bacteria use memory. *Biol. Chem.* **390**, 1097–1104 (2009).
42. Lazova, M. D., Ahmed, T., Bellomo, D., Stocker, R. & Shimizu, T. S. Response rescaling in bacterial chemotaxis. *Proc. Natl. Acad. Sci. U.S.A.* **108**, 13870–13875 (2011).
43. Kamino, K. & Kondo, Y. Rescaling of spatio-temporal sensing in eukaryotic chemotaxis. *PLoS ONE* **11**, e0164674 (2016).
44. Min, T. L., Mears, P. J., Golding, I. & Chemla, Y. R. Chemotactic adaptation kinetics of individual *Escherichia coli* cells. *Proc. Natl. Acad. Sci. U.S.A.* **109**, 9869–9874 (2012).
45. Shimizu, T. S., Tu, Y. & H. C: Berg,. A modular gradient-sensing network for chemotaxis in *Escherichia coli* revealed by responses to time-varying stimuli. *Molecular Systems Biology* **6**, 382 (2010).
46. Springer, M. S., Goy, M. F. & Adler, J. Protein methylation in behavioral control mechanisms and in signal transduction. *Nature* **280**, 279–284 (1979).
47. Minamino, T., Imae, Y., Oosawa, F., Kobayashi, Y. & Oosawa, K. Effect of intracellular pH on rotational speed of bacterial flagellar motors. *Journal of Bacteriology* **185**, 1190–1194 (2003).
48. Paul, K., Nieto, V., Carlquist, W. C., Blair, D. F. & Harshey, R. M. The c-di-GMP binding protein YcgR controls flagellar motor direction and speed to affect chemotaxis by a "backstop brake" mechanism. *Molecuar Cell* **38**, 128–139 (2010).
49. Mowbray, S. L. & Koshland, D. E. Additive and independent responses in a single receptor: Aspartate and maltose stimuli on the tar protein. *Cell* **50**(2), 171–180 (1987).
50. Mao, X., Egli, R., Liu, X. & Zhao, L. Magnetotactic advantage in stable sediment by long-term observations of magnetotactic bacteria in Earth's field, zero field, and alternating field. *PloS ONE.* **17**(2), e0263593 (2022).
51. Egbert, M. D., Barandiaran, X. E. & Di Paolo, E. A. A minimal model of metabolism-based chemotaxis. *PLoS Computational Biology* **6**, e1001004 (2010).
52. Lin, W. et al. Origin of microbial biomineralization and magnetotaxis during the Archean. *Proceedings of the National Academy of Sciences.* **114**, 2171–2176 (2017).

Acknowledgements

This work is supported by National Natural Science Foundation of China (Grant No. 41602184, 42130507, 41772180), Natural Science Foundation of Fujian Province (Grant No. 2020J01141), and German Research Foundation (Grant No. EG 294/1-1 and EG 294/2-1). We are grateful to the associated editor and three anonymous reviewers for their insightful comments.

Author contributions

X. M. and R. E. conducted the experiments. X. M, R. E., N. P., and X. L. analyzed of the data., X. M., R.E. and N.P. made the modeling. X.M. and R.E. wrote the paper. R.E. and X. L. supervised the work.

Declarations

Competing interests

The authors declare no competing interests.

Additional information

Supplementary Information The online version contains supplementary material available at https://doi.org/10.1038/s41598-024-78946-7.

Correspondence and requests for materials should be addressed to X.M. or R.E.

Reprints and permissions information is available at www.nature.com/reprints.

Publisher's note Springer Nature remains neutral with regard to jurisdictional claims in published maps and institutional affiliations.